



## Time-Domain Measurements of Reflection Delay in Frustrated Total Internal Reflection

George M. Gehring,<sup>1</sup> Andreas C. Liapis,<sup>1</sup> Svetlana G. Lukishova,<sup>1</sup> and Robert W. Boyd<sup>1,2,3</sup>

<sup>1</sup>*The Institute of Optics, University of Rochester, Rochester, New York 14627, USA*

<sup>2</sup>*Department of Physics and Astronomy, University of Rochester, Rochester, New York 14627, USA*

<sup>3</sup>*Department of Physics and School of Electrical Engineering and Computer Science, University of Ottawa, Ottawa, Ontario K1N 6N5, Canada*

(Received 9 April 2013; published 18 July 2013)

We present experimental evidence that the contribution of the Goos-Hänchen shift to tunneling delay is suppressed in frustrated total internal reflection. We use a Hong-Ou-Mandel interferometer to perform direct time measurements of reflection delays with femtosecond resolution at optical frequencies, and take advantage of a liquid-crystal-filled double-prism structure to dynamically change the refractive index of the barrier region.

DOI: [10.1103/PhysRevLett.111.030404](https://doi.org/10.1103/PhysRevLett.111.030404)

PACS numbers: 03.65.Xp, 41.20.Jb, 42.25.Gy

The measurement of tunneling times in one-dimensional quantum-mechanical systems lies at the heart of the understanding of many quantum mechanical phenomena. It is commonly accepted that time delays in frustrated total internal reflection (FTIR) represent an optical analog to these quantum-mechanical tunneling times due to the formal similarity of the Helmholtz and Schrödinger equations. A number of authors have addressed this analogy over the last 25 years, focusing primarily on glass-air-glass double-prism structures [1–3]. Foremost amongst the discussion are the questions of what exactly causes the time delay experienced by a photon undergoing FTIR and what time delay one would observe experimentally in such a system [4]. One would expect that the Goos-Hänchen shift would make a sizable contribution to the measured time delay. Nonetheless, in this Letter we present experimental evidence that the contribution of the Goos-Hänchen shift is in fact negligible in this two-dimensional tunneling system.

Direct measurements of time delays in FTIR are difficult to make, leading researchers to choose easier, indirect methods of measurement. The delay experienced by a photon undergoing FTIR can be inferred in an indirect manner by measuring other observable quantities that are correlated to delay values according to theory. In [5], the authors utilized an optical analog to the Larmor clock proposed by Büttiker [6] and inferred a Larmor-like tunneling delay based on the Stokes parameters of the tunneled beam. However, they note that the strong anisotropy in their system prevents them from unambiguously determining the Larmor time as a traversal time, and that it is still an open question whether the Büttiker treatment, which gives a complex time delay, has a significant physical meaning [7,8].

Balcou and Dutriaux [9] instead focus on the Goos-Hänchen shift  $\Delta y$  and the deviation in output angle caused by the selective frequency transmission of FTIR. From accurate position and angle measurements, the authors

infer the tunneling delay times in both reflection and transmission. Their measurement of  $\Delta y$  seems to confirm the “phase time” predictions of Hartman and others [10], while the measurement of deviation of output angle agrees with the “loss time” suggested by Büttiker’s treatment. They also observed that the “phase time” was symmetric in transmission and reflection but depended on the boundary conditions, while the “loss time” was heavily asymmetric in transmission and reflection but showed no dependence on the boundary conditions. They contend that this makes the “loss time” the more relevant measure of time spent within the barrier, though there are significant criticisms of this formulation [7].

In addition, it is our feeling that their conclusion overlooks the fact that boundary conditions do have a significant effect on the time spent in the barrier region, as a different boundary condition corresponds to a different effective barrier height and wave function presence in the barrier region. It should be no more surprising that the “phase time” measurement saturates to a different value for TE- and TM-polarized photons than that it saturates to different values for different barrier heights.

We have explicitly calculated the expected group delay in a double-prism FTIR structure using a formulation that treats the problem as an evanescent cavity lifetime [11]. Our method properly accounts for the coupling into and out of the prism pair [12], a detail that appears to have been overlooked or omitted in the majority of the literature [1,3,13–16], which has led some researchers to inaccurate conclusions. In this Letter, we present our experimental measurements of tunneling delay in reflection from a double-prism FTIR structure. These measurements confirm that the calculations of “measurable delay” in [12] are accurate.

A double-prism structure as proposed by Steinberg and Chiao [2] is difficult to achieve experimentally, because it requires fine control of the subwavelength air gap distance between two large-surface-area interfaces. However, the

tunneling process is governed by  $\kappa L$ , the barrier “opacity.” Thus, instead of increasing the barrier length, we can consider increasing the “height” by changing  $\kappa$ . We have chosen this approach for our experiment, modulating the barrier height by introducing a liquid crystal (LC) into the barrier region. The LC molecular director can be tuned by an externally applied voltage to change the index contrast of the glass-LC interface and consequently the effective barrier height. Our system also has no moving parts and does not introduce significant beam deviations during the tuning process, both of which are liabilities inherent to mechanically tuned devices.

Our experimental implementation of a double-prism system is shown in Fig. 1. A planar-aligned nematic LC cell is sandwiched between two equilateral prisms. The cell substrates and prisms are made of high-index N-SF11 glass, which has a refractive index of  $n = 1.77$  at  $\lambda = 727$  nm. Index-matching fluid ( $n = 1.70$ ) is applied to the prism-cell interfaces to minimize reflections.

Cell preparation is a multistage process that occurs in a cleanroom environment. Two 3-mm thick N-SF11 substrates are sputter-coated with a 30-nm layer of indium tin oxide (ITO) to serve as an electrode. Next, an approximately 15-nm alignment layer of polyimide solution is spin-coated on top of the ITO layer. The alignment layer is subjected to a mechanical buffing technique that structures the polyimide layer, causing the LC director to align along the buffing direction when the cell is filled [17]. The cell is then constructed by creating spacers between the two processed faces using a mixture of 5-minute epoxy and 5- $\mu\text{m}$  glass beads and applying pressure while the epoxy mixture cures. Spectrophotometer measurements suggest that the void thickness in cells prepared with this technique is approximately 8–12  $\mu\text{m}$ .

The cell is then filled with Merck E7 LC mixture through capillary action. E7 is a uniaxial nematic LC mixture ( $n_e = 1.718$  and  $n_o = 1.514$  at  $\lambda = 727$  nm [18]) which is popular, commercially available, and relatively inexpensive. The edges of the cell are sealed with epoxy after filling to prevent evaporative loss and deterioration of the LC. Wires are attached to the exposed ITO

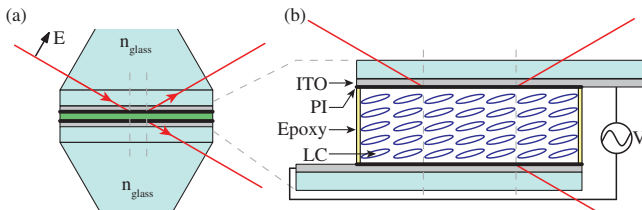


FIG. 1 (color online). Diagram of the double-prism system. In (a) a liquid crystal cell is sandwiched between two glass equilateral prisms. An exploded diagram of the liquid crystal cell is shown in (b), with the liquid crystal (LC), indium tin oxide (ITO) layer and polyimide alignment (PI) layer labeled.

sections with conductive silver epoxy to enable electronic control of the orientation of the LC director and subsequently modify its optical properties [19].

The dependence of LC molecular director rotation angle to an applied 1 kHz ac voltage is empirically determined from transmission measurements with a method described in [20]. At oblique incidence, tuning of the LC director angle is equivalent to tuning the critical angle of the glass-LC interface. The relevant indices of E7 and N-SF11 dictate a range of achievable critical angles from  $58.5^\circ$  to  $76.1^\circ$ . Thus, the desired angle of incidence is between  $60^\circ$  and  $65^\circ$  such that we can make measurements in both the FTIR and Fabry-Perot regimes by tuning the critical angle of the structure. We employ equilateral prisms as a coupling aid to achieve the appropriate angle in the glass region.

The experimental setup is shown in Fig. 2. The pump source is a continuous-wave Coherent Innova Sabre argon-ion laser operating at 363.8 nm, producing up to 1 W of power with a linewidth of approximately 3 GHz. This laser pumps a 3-mm BBO crystal to generate time-entangled photons at 727 nm by Type I noncollinear spontaneous parametric down-conversion (SPDC). The crystal is aligned and angle-tuned such that the generated photons are emitted in a cone with a half-angle of approximately 0.1 radians. The pump beam is focused on the crystal to increase the SPDC generation rate.

The two down-converted photons then proceed through different arms of the interferometer. A small 10-cm focal length lens is placed in each arm about

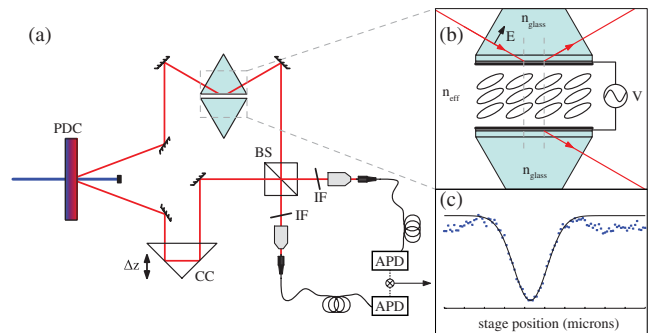


FIG. 2 (color online). Abbreviated setup diagram showing FTIR measurements in the reflection geometry. Panel (a) shows the Hong-Ou-Mandel arrangement and placement of components. PDC is the parametric down-conversion crystal, CC is a corner cube retroreflector, BS is a nonpolarizing 50/50 beam splitter, IF are 10-nm bandpass interference filters centered at 727 nm, APD are avalanche photodiode single-photon counting modules. Inset (b) shows a detailed view of the FTIR region, with two prisms of index  $n_{\text{glass}}$  and a barrier region of liquid crystals with an effective index  $n_{\text{eff}}$  due to the applied voltage  $V$ . Inset (c) shows an example data trace containing a Hong-Ou-Mandel dip, along with a numerical Gaussian fit.

20 cm from the down-conversion crystal. This keeps the beam size small (1 mm diameter) near the interaction region of the prism structure, minimizing LC nonuniformity and preventing the mode size from growing so large that it overfills the microscope objectives in the collection arms.

The lower arm contains a “trombone” system consisting of a corner cube retroreflector mounted on a motorized linear translation stage (Aerotech model AT550-25-M-2). This system introduces a controllable amount of path delay for the photon in the lower arm. The photon in the upper arm is incident on the double-prism test system at an angle of approximately  $6^\circ \pm 1^\circ$  to the prism face normal, corresponding to an internal glass-LC incidence angle of approximately  $63.5^\circ$ .

The two arms of the interferometer are then brought back together at a nonpolarizing 50/50 beam splitter to create a Hong-Ou-Mandel (HOM) interferometer [21]. The beam splitter’s outputs are passed through 10-nm band-pass filters centered at 727 nm to suppress pump fluorescence and ambient light. The transmitted light is then coupled into single-mode optical fiber and sent to avalanche photodiode (APD) single-photon counting modules (PerkinElmer SPCM-AQR-14-FC). These modules have very low dark count rates (less than 100 counts per second) and a quantum efficiency of approximately 70% at 727 nm.

Coincidence circuitry tracks the number of individual (“singles”) events at each detector as well as the number of coincidence events. The circuit is homebuilt and based on a design published by Mark Beck [22] which is freely available online [23]. The discrimination time window of the circuit is nominally about 12–15 nanoseconds, which is sufficiently large to guarantee that any generated pair of entangled photons which successfully triggers both APDs will be counted. The width of this window also ensures that odd-order dispersion effects (including group velocity dispersion) cancel out and do not artificially broaden the HOM dip [24].

Measurements are made over a 50-micron range of stage movement in 1-micron increments. At each stage position we record the LC voltage, integration time, singles counts on each detector, and coincidence counts. An experimental data run involves performing a large number of HOM traces with different voltages applied to the LC. Data collection alternates between traces taken at a sample voltage and traces taken at a reference voltage ( $V_r = 0$  volts) to help track and eliminate errors caused by mechanical and thermal drifts in the setup.

Once the coincidence data have been collected, it goes through several postprocessing steps to extract accurate values for the FWHM, position, and visibility of the dip for a given trace or set of traces. Each trace is fitted to a Gaussian function using a nonlinear least squares method to accurately extract the position of the HOM

minimum, from which our delay values are calculated. Pairing these delay values with the associated LC voltages gives us the relationship between applied voltage and path delay.

Since our experiment contains no absolute reference, all of our measurements are necessarily relative delays, or measured centroid differences between the reference voltage and a sample voltage. As such, we cannot make statements about absolute delays or superluminality from our data. We can, however, characterize the delay curves as a function of voltage or LC director angle and compare them to the theoretical predictions for our system to determine whether the model of tunneling is accurate.

Figure 3 shows the results of our measurements in the reflection geometry. Four sets of data are shown, each of which contains 176 data points representing individual HOM traces. For each trace, coincidence was measured at 51 stage positions for 2 seconds, giving a total integration time per trace of 102 seconds. The black line represents the arithmetic mean of all four data points at each position. All delay measurements are relative to the delay observed at the reference voltage.

We have simulated the expected delay using a  $4 \times 4$  matrix method [25] which solves Maxwell’s equations in matrix form for our multilayer slab structure. This technique calculates the complex transmission and reflection coefficients for a given LC director orientation, photon frequency, and incidence angle. Since this method assumes plane wave incidence, we have convolved the phase  $\Phi_R$  of the reflection coefficient with a Gaussian function to account for the spread of incidence angles present in our Gaussian beam and the effects of LC disorder.

The reflection delay  $\partial\Phi_R/\partial\omega$  predicted by the simulation is shown in Fig. 4 for LC voltages ranging from 1.5 V to 5 V, corresponding to LC director angles of  $69.3^\circ$  to  $18.3^\circ$ , respectively, as measured from the cell normal. In this simulation the light is incident at  $63.5^\circ$  from N-SF11 glass ( $n_{\text{N-SF11}} = 1.77$ ) on an 8- $\mu\text{m}$ -thickness LC cell. The extraordinary and ordinary refractive indices used for the LC are  $n_e = 1.63$  and  $n_o = 1.54$ . These indices are a little lower and higher, respectively, than the expected values for the E7 LC used in our experiment to correct for LC disorder. The chosen cell thickness is a little thinner than the nominal value of 12  $\mu\text{m}$  inferred from spectrophotometric measurements. However, these parameters primarily affect the spacing and magnitude of the Fabry-Perot fringes observed, and were chosen for better agreement with our experimental data.

The experimental data are in excellent agreement with the model predictions for experimentally measured group delay  $\tau_{\gamma,\text{meas}}$  [12], making it clear that the  $\Delta y$  contributions to the delay truly are suppressed in this type of measurement. The delay in the tunneling region (below

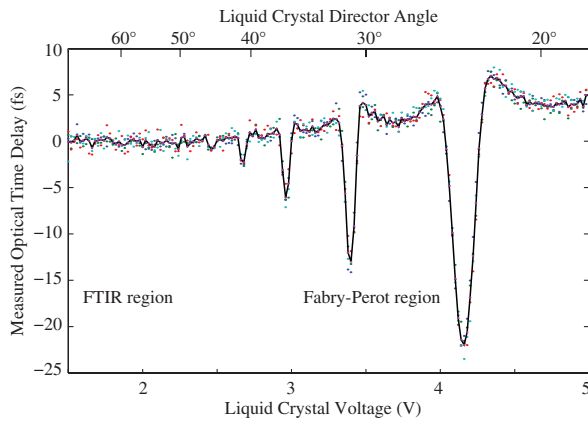


FIG. 3 (color online). Reflection delay in FTIR from a double-prism barrier system. The black line is the arithmetic mean of four individual data sets, shown in colored dots. Each data point represents an individual Hong-Ou-Mandel trace with 102 seconds of integration time.

approximately 2.2 V) appears to be identically zero within the experimental uncertainty, observed to be approximately  $\pm 1$  fs or less. Measurements below 1.5 V were consistent with these results as well, though they have been omitted from the plot for clarity. In the Fabry-Perot region, we observe the sharp dips at each resonance corresponding to interference from the Gaussian beam  $k$ -vector distribution as well as the slowly increasing delay predicted between resonances. The sharp dips are not as pronounced as those shown in Fig. 4 because the simulation only addresses the phase of the reflection coefficient. In experiment, the amplitude of the reflection coefficient is smaller at the Fabry-Perot resonances than when off-resonant, leading to an uneven weighting that reduces the magnitude of the dips in the measured delay.

In this Letter, we have presented single-photon time delay measurements in a double-prism FTIR structure. These measurements confirm our earlier theoretical predictions that the Goos-Hänchen contribution is suppressed in the measurable portion of the tunneling delay in this geometry [12]. The fact that this contribution is suppressed may prove important for practical devices [26,27]. In addition, these are the first direct time measurements of FTIR tunneling delay at optical frequencies.

These results strongly support the cavity interpretation presented by Winful [11], who emphasizes the quasistatic nature of the tunneling process. The group delay should be interpreted as a cavity lifetime rather than a transit time. As such, it can become shorter than the “equal time”  $c/L$  without violating causality. Moreover, the use of single photons disqualifies alternative explanations of the Hartman effect that rely on nonlinear effects or preferential transmission of photons in the leading edge of a multiphoton pulse. Follow-up measurements with a thinner cell to confirm the model’s transmission predictions should further support this interpretation.

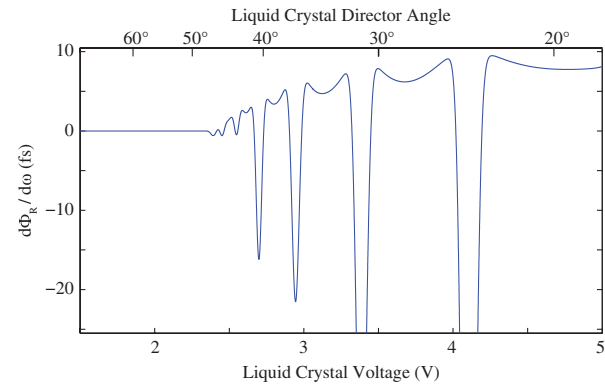


FIG. 4 (color online). Predicted  $\partial\Phi_R/\partial\omega$  based on the  $4 \times 4$  matrix method described in the text for 727-nm light propagating through an 8-micron liquid crystal cell. The parameters used are  $\theta = 63.5^\circ$ ,  $n_{\text{glass}} = 1.77$ ,  $n_e = 1.63$ , and  $n_o = 1.54$ .

We acknowledge the assistance of Kenneth Marshall and Simon Wei in constructing the LC cells used in the experiment. S. G. L. is supported by the NSF (Grant No. DUE-0920500). This work was supported by the US Defense Threat Reduction Agency—Joint Science and Technology Office for Chemical and Biological Defense (Grant No. HDTRA1-10-1-0025) and by the Canada Excellence Research Chairs Program.

- [1] A. Ghatak and S. Banerjee, *Appl. Opt.* **28**, 1960 (1989).
- [2] A. M. Steinberg and R. Y. Chiao, *Phys. Rev. A* **49**, 3283 (1994).
- [3] B. Lee and W. Lee, *J. Opt. Soc. Am. B* **14**, 777 (1997).
- [4] K. Resch, J. Lundeen, and A. M. Steinberg, *IEEE J. Quantum Electron.* **37**, 794 (2001).
- [5] M. Deutsch and J. E. Golub, *Phys. Rev. A* **53**, 434 (1996).
- [6] M. Büttiker, *Phys. Rev. B* **27**, 6178 (1983).
- [7] S. Collins, D. Lowe, and J. R. Barker, *J. Phys. C* **20**, 6213 (1987).
- [8] E. Pollak and W. H. Miller, *Phys. Rev. Lett.* **53**, 115 (1984).
- [9] P. Balcou and L. Dutriaux, *Phys. Rev. Lett.* **78**, 851 (1997).
- [10] T. E. Hartman, *J. Appl. Phys.* **33**, 3427 (1962).
- [11] H. G. Winful, *Phys. Rev. Lett.* **91**, 260401 (2003).
- [12] G. M. Gehring, A. C. Liapis, and R. W. Boyd, *Phys. Rev. A* **85**, 032122 (2012).
- [13] R. Chiao, P. Kwiat, and A. M. Steinberg, *Physica (Amsterdam)* **175B**, 257 (1991).
- [14] A. Haibel and G. Nimtz, *Ann. Phys. (Berlin)* **10**, 707 (2001).
- [15] G. Nimtz and A. Haibel, *Ann. Phys. (Berlin)* **11**, 163 (2002).
- [16] D. J. Papoular, P. Clade, S. V. Polyakov, C. F. McCormick, A. L. Migdall, and P. D. Lett, *Opt. Express* **16**, 16005 (2008).
- [17] J. M. Geary, J. W. Goodby, A. R. Kmetz, and J. S. Patel, *J. Appl. Phys.* **62**, 4100 (1987).
- [18] J. Li, C.-H. Wen, S. Gauza, R. Lu, and S.-T. Wu, *J. Disp. Technol.* **1**, 51 (2005).
- [19] I.-C. Khoo, *Liquid Crystals* (Wiley-Interscience, Hoboken, NJ, 2007), 2nd ed., p. 368.

- [20] S.-T. Wu, U. Efron, and L. D. Hess, *Appl. Opt.* **23**, 3911 (1984).
- [21] C. K. Hong, Z. Y. Ou, and L. Mandel, *Phys. Rev. Lett.* **59**, 2044 (1987).
- [22] D. Branning, S. Bhandari, and M. Beck, *Am. J. Phys.* **77**, 667 (2009).
- [23] M. Beck, and D. Branning, “Coincidence Counting Units (CCUs),” <http://people.whitman.edu/beckmk/QM/circuit/circuit.html> (2011).
- [24] A. M. Steinberg, P. G. Kwiat, and R. Y. Chiao, *Phys. Rev. A* **45**, 6659 (1992).
- [25] D. W. Berreman, *J. Opt. Soc. Am.* **62**, 502 (1972).
- [26] S. G. Lukishova, P. P. Pashinin, S. K. Batygov, V. A. Arkhangelskaya, A. E. Poletimov, A. S. Scheulin, and B. M. Terentiev, *Laser Part. Beams* **8**, 349 (1990).
- [27] A. Q. Jian and X. M. Zhang, *IEEE J. Sel. Top. Quantum Electron.* **19**, 9000310 (2013).